

Receiver Depth Selection for Passive Sonar Systems

Carlo M. Ferla and Michael B. Porter

Abstract—Tactical acoustic systems such as towed arrays may, in general, be deployed at various depths, which raises the question of what depth is optimal. We address this question principally from the point of view of optimum propagation conditions employing two deep-water scenarios representing summer and winter conditions in the western Mediterranean. Two simple “rules-of-thumb” may be derived from these results: First, if the source depth is known, then the best receiver depth is either the source depth or the conjugate depth (where the sound speed is the same as that at the source). Second, if the source depth is unknown, then a receiver depth where the ocean sound speed is as low as possible is optimal. These two rules, which already enjoy a certain currency in tactical doctrine, must be footnoted with a few disclaimers. In the first place they are derived under the assumption of a range-invariant environment. In addition, a definition of optimality requires numerous assumptions that may not always be appropriate. We discuss both these guidelines and their domain of applicability.

I. INTRODUCTION

THE question of choosing an optimal depth for an acoustic system arises in several contexts, e.g., surface and submarine towed arrays and submarine bow sonar. The decision may be a permanent design consideration or a tactical decision—we imagine in the latter case a surface ship towed array that can be deployed at different depths. The question is relevant for both active and passive systems; however, we consider only the latter case here.

In order to address this issue, we have selected environmental data representing summer and winter conditions in a western Mediterranean site (the Balearic Sea). Both low (50 Hz) and high (600 Hz) frequencies have been considered. Transmission loss plots were computed for a sequence of plausible source depths in the upper 500 meters. Next, a “detection radius” was introduced as a measure of how well an array might perform at some particular deployment depth. While the numerical values are specific to the particular site, the thrust of this work is to identify the general features that are important, especially from the point of view of ideal propagation conditions. The Mediterranean data is merely intended to be an illustrative example. (We should also like to mention that the shallow-water case poses special problems but has been studied in detail by Gershfeld and Ingenito [1]).

One of the most difficult questions in such a study is to provide a useful definition of what constitutes an optimal

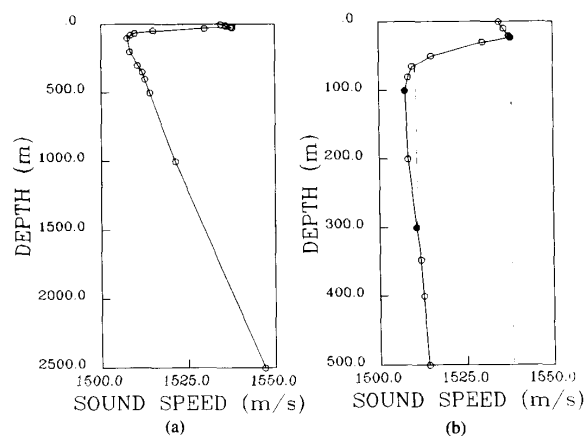


Fig. 1. Sound speed profile in the Mediterranean site during the summer. (a) Full water column., (b) Blow-up of upper 500 m.

depth. Problems to consider include the following: 1) Are detections at all ranges equally important, 2) Is it adequate to optimize for signal level or must one consider signal to noise, 3) What information shall we suppose we know in advance, specifically, might we know source depth? Certain assumptions are made in the first sections about these questions; however, we return to these issues in the final discussion and conclusions.

The outline of this paper is as follows. In Section II, we consider the case where the source depth is known. Particular subsections provide a description of the environmental conditions, the criterion for defining an optimal depth, and interpretation of the results. In Section III, we consider the case where the source depth is assumed to be essentially unknown, i.e., somewhere in the upper 500 meters. In Section IV we discuss the simplifying assumptions inherent in our processing, and finally, in Section V, we summarize our conclusions. The latter are necessarily limited by the assumptions used in the analysis but, nevertheless, we believe will be valid in the majority of deep-water scenarios.

II. THE CASE OF KNOWN SOURCE DEPTH

2.1. Environment (Summer Profile)

For the purpose of this study, we have taken environmental data from a site in the western Mediterranean (Balearic sea). A plot of the sound-speed profile taken in the summer is shown in Fig. 1. We will be showing results for a sequence of source depths (25 m, 100 m, and 300 m), which are

Manuscript received February 2, 1991.
The authors are with the Saclant Undersea Research Centre, Viale San Bartolomeo 400, I-19026 La Spezia, Italy.
IEEE Log Number 9143375

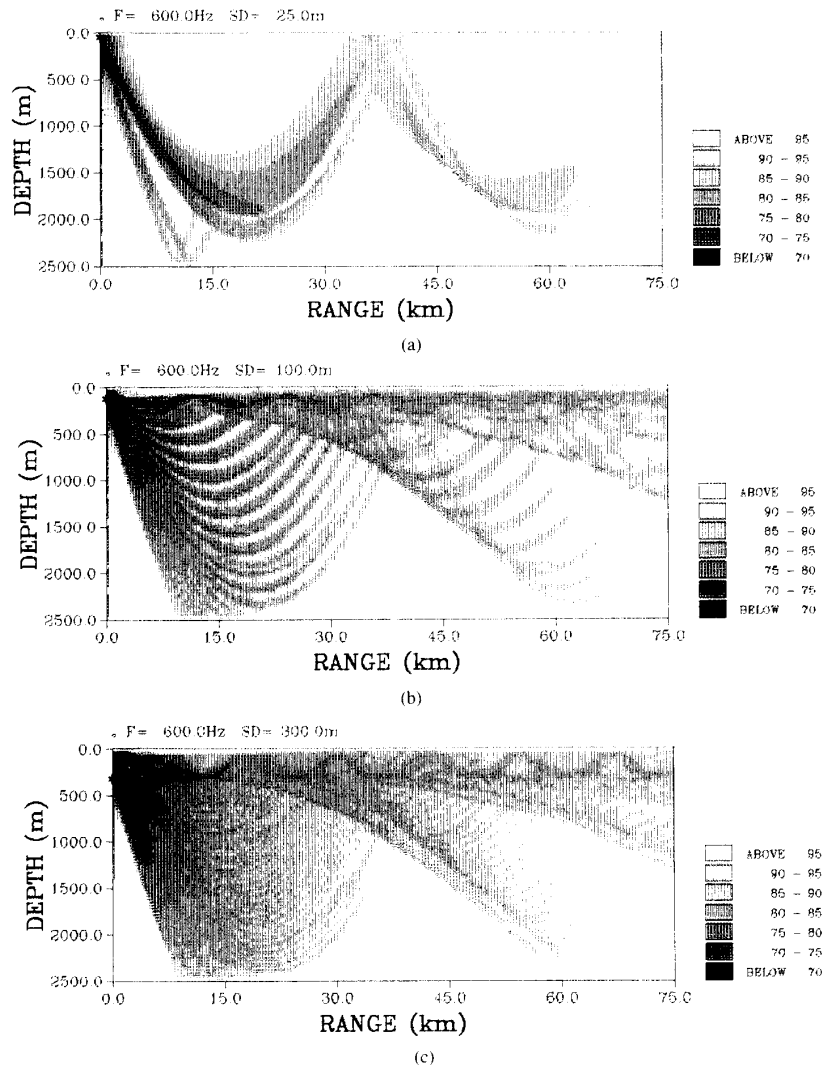


Fig. 2. Transmission loss plots for the summer profile and a 600 Hz source at depths (a) 25 m, (b) 100 m, (c) 300 m.

indicated by solid circles. The summer profile manifests higher sound speeds near the surface reflecting the increase in water temperature. The ocean bottom consists of a thick (200 m) sediment overlying a faster sub-bottom, which, for modeling purposes, is replaced by a homogeneous half-space. Scattering at the ocean surface is modeled using the Kuperman-Ingenito model [2] with an RMS roughness of 0.5 m, which corresponds to sea state 4.

In Fig. 2 we display transmission loss plots for a sequence of source depths (25 m, 100 m, and 300 m) and a source frequency of 600 Hz. These results are obtained using the SUPERSNAP normal mode code [3], which provides full-wave solutions quite efficiently for such range-independent environments—approximately 10 min of CPU time on a VAX 8600 were required to produce the sequence of plots in Fig. 2.

For the shallowest source we see a typical deep-water convergence zone (CZ) pattern involving a band of water-borne energy cycling up and down the channel. Between the CZ's we find "shadow zones" where the only contribution is from bottom bounce energy. The bottom-bounce energy loses strength with every bottom interaction, so that it is most important in the first 50 km or so, depending on frequency and bottom characteristics. At 600-Hz energy is dissipated rapidly in the sediment—the degree of sediment attenuation is reflected in Fig. 2(a) by the relatively low levels of the bottom bounce paths.

The occurrence of a fan of beams emanating from the omnidirectional source is due to the interference of direct and surface reflected energy, in the near-field this yields the classical "Lloyd mirror" pattern with the number of lobes depending on the distance the source is from the surface. We

observe that the waterborne energy dominates the field except for the shallow source case where, in ray terms, the Lloyd mirror pattern directs more energy towards the bottom. Note also the significant change in the field structure as the source depth increases—the classical convergence zone pattern gives way to a structure in which there are no shadow zones and hence no gaps in the coverage. (This transition will generally occur in deep-water profiles but may be more gradual in the Pacific or Atlantic especially in low latitudes where the sound channel is deeper.)

2.2. Optimal Receiver Depth

Referring to the transmission loss plot in Fig. 2(a), we see that there are some trade-offs involved in selecting the optimal receiver depth. There are loud spots where the source is most easily detected that occur at the source depth and repeat at the convergence zones, every 35 km or so. On the other hand, by placing the array deeper, the bands of energy cover wider zones, which extend slightly further in range. Wider zones suggest longer observation times and improved detection performance.

In order to make some quantitative comparisons between these possible receiver depths, we apply two transforms to the data. First we will associate the transmission loss with a “probability of detection” (p_D) and secondly we will identify the optimal receiver depth as the depth where the p_D is highest in a range-integrated sense.

To be precise, we will assume that the probability of detection is given by a log-normal distribution:

$$p_D(\text{SE}) = \frac{1}{\sqrt{2\pi}\sigma} \int_{-\infty}^{\text{SE}} \exp\left[-\frac{x^2}{2\sigma^2}\right] dx \quad (1)$$

where SE is the signal excess representing the degree to which the source stands out above the noise background with an SE of 0 dB implying a 50% probability of detection. The signal excess is computed by first obtaining a figure of merit (FM) for the source that takes into account the source level (SL), the noise level (NL), the directivity index of the array (DI), and a detection threshold (DT), and then by subtracting the transmission loss (TL) from the source to the receiver. That is,

$$\text{FM} = \text{SL} - \text{NL} + \text{DI} - \text{DT} \quad (2)$$

and

$$\text{SE}(\text{FM}, r, z_r | z_s) = \text{FM} - \text{TL}(r, z_r | z_s). \quad (3)$$

The FM is assumed to be a given constant, while the TL depends on source depth z_s , receiver depth z_r , and source/receiver separation r . A plot of the probability of detection versus SE is provided in Fig. 3. The sharpness of the transition from non-detection to detection is a function of σ , which is set at 8 dB in our computations. We refer the reader to Urick [4] for more information on this calculation.

With a given FM we may thus convert a transmission loss surface into a p_D surface, an example of which is provided in Fig. 4. This p_D surface is computed assuming an FM of 80 dB and for the source depth and frequency used in Fig.

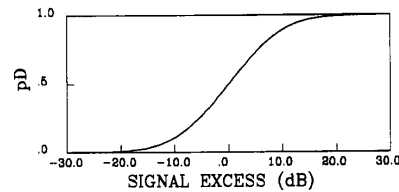


Fig. 3. Assumed probability of detection versus signal excess (transition curve) for $\sigma = 8$ dB.

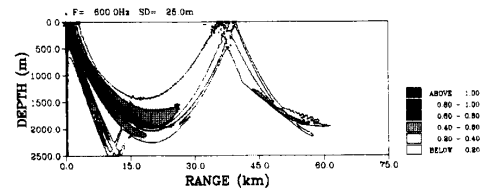


Fig. 4. Probability of detection plot for the 600-Hz shallow source.

2(a). Note that the pattern is roughly the same as in Fig. 2(a); however, the numerical values are different. In order to make comparisons between different p_D surface we define a detection radius as the range-integrated probability of detection:

$$R(\text{FM}, z_r | z_s) = \int_0^{\infty} p_D(\text{FM}, r, z_r | z_s) dr. \quad (4)$$

We caution that this detection radius does not imply some expected range at which a source will be detected but is just a simple measure of how well the range axis is covered.

2.3. Implications (Summer Profile, 600 Hz)

In Fig. 5 we provide plots of the detection radius as a function of receiver depth and FM for each of the three source depths. (The vertical axis is restricted to the upper 500 m of the water-column representing a domain of plausible deployment depths.) Examining the result for the source at 100 m in Fig. 5(b), we see that there is a strong peak that occurs when the receiver is deployed at the source depth. We can read the graph in different ways, e.g., for a fixed detection radius we can follow a contour to see the corresponding FM that yields that radius. Thus, reading some numbers off the plot, a detection radius of 50 km requires only an FM of about 75 dB for an array at the source depth. An array deployed at 50 m would require an FM of about 87 dB for the same detection radius. Alternatively, given an FM of say 80 dB the detection radius increases from about 20 km to 80 km as we increase the receiver depth from 50 m to the source depth at 100 m.

Two characteristics are illustrated by these plots of the radius of detection: *The detection radius is generally greatest when the receiver is deployed at the same depth as the source or at the conjugate depth.* (We refer the reader back to Fig. 1 for the positions of the source and conjugate depths.) Thus, in Fig. 5(a), the peak is at the source depth. A conjugate depth occurs close to the ocean bottom and so is of no relevance for an array restricted to the upper 500 m. In Fig. 5(b) the source depth is at 100 m, which is precisely at the sound channel axis. Here, the source depth and conjugate

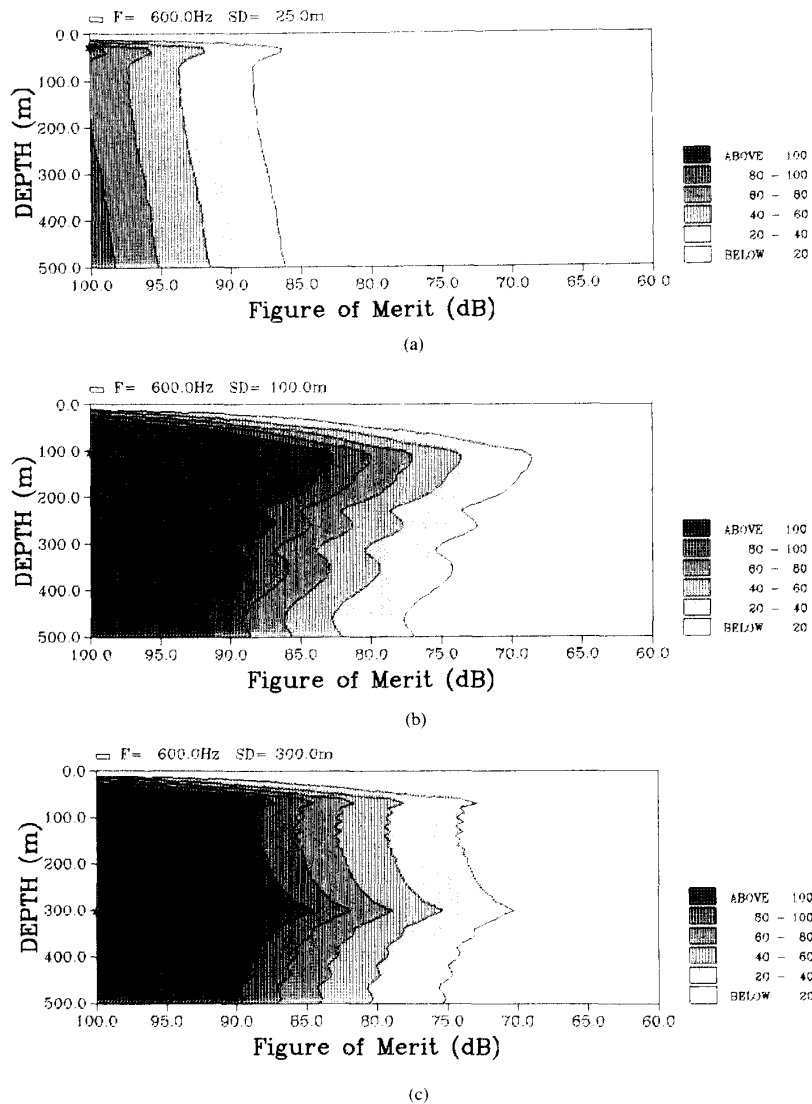


Fig. 5. Detection radius for the summer profile and a 600-Hz source at depths (a) 25 m, (b) 100 m, and (c) 300 m.

depth have coalesced leaving a single optimal receiver depth. Finally, in Fig. 5(c) the source depth is increased to 300 m so that now the conjugate depth is above the source depth, at approximately 60 m. Now, two good receiver depths are present, one at the source depth and the other at the conjugate depth.

2.4. Summer Profile, 50 Hz

We now turn to the low-frequency regime (50 Hz) obtaining the sequence of transmission loss plots and detection radii shown in Figs. 6 and 7, respectively. Looking first at the transmission loss plots, we observe that the low-frequency plots differ from the high-frequency case in the absence of shadow zones. This is a consequence of the reduced sediment attenuation at lower frequencies, which enables sediment-re-

fracted energy to return to the water column with significant intensity. In addition, the Lloyd mirror pattern shows fewer lobes since the source is closer in wavelengths to the surface.

The sequence of plots of detection radii in Fig. 7, show a somewhat muted version of the same features we saw in the high-frequency case. The source and conjugate depths remain as reasonable receiver depths, but for the shallower source depth (25 m) corresponding to Fig. 7(a), the detection radius is roughly constant over a certain zone. This region is defined by points where the sound speed is less than the source sound speed. For the deeper sources (100 m and 300 m) the source depths emerge again as favorable depths. For the 300-m source, there is also a peak roughly at the conjugate depth. In summary, the source-depth/conjugate-depth choice is still good but it is generally less critical.

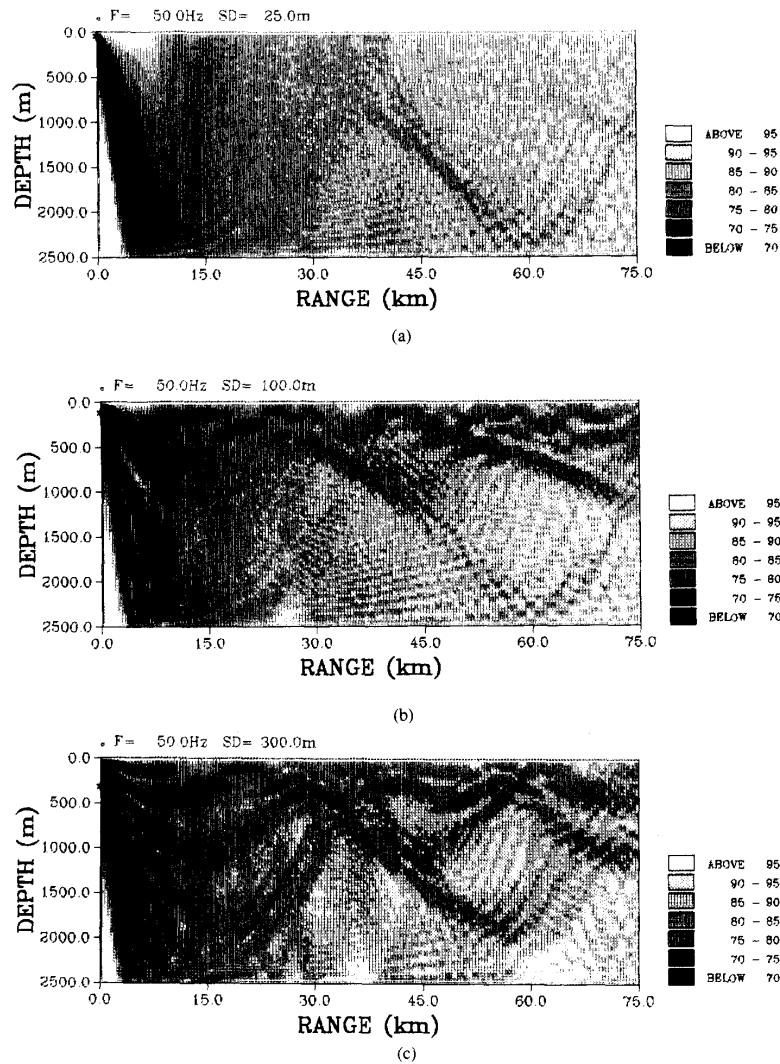


Fig. 6. Transmission loss plots for the summer profile and a 50-Hz source at depths (a) 25 m, (b) 100 m, and (c) 300 m.

2.5. Winter Profile

As a final example we consider the same site in the western Mediterranean but with a sound speed profile taken in the winter. The particular sound-speed profile is indicated in Fig. 8. Note that the sound speed increase monotonically with depth so that there are no conjugate depths.

The effect of this new sound speed profile on transmission loss is indicated in Fig. 9 for a 600-Hz source. Compared to the high-frequency summer profile plots, the biggest difference shows up for the shallow source: the convergence zone pattern is essentially eliminated so that no shadow zones occur. In Fig. 10, we provide plots of the detection radius for the usual sequence of depths, 25 m, 100 m, and 300 m. As expected, the peak in detection radius again occurs when the receiver depth matches that of the source.

Comparing these results to the summer profile case we note that again the biggest difference shows up for the near-surface source. The detection radius is significantly less for the same FM for the summer profile. This is essentially a seasonal version of the "afternoon effect." For the deeper sources the situation is somewhat reversed: the summer profile yields a slightly larger detection radius. This is because surface scatter plays a lesser role when the warm surface layer turns the upgoing rays away from the surface.

In summary, the winter environment, though substantially different in terms of the sound-speed profile, manifests the same feature of a peak at the source depth. We have performed simulations in several different environments, including a thinly sedimented Pacific case and an Arctic scenario, which collectively provide a sense that the source-depth/conjugate-depth peak is a robust feature.

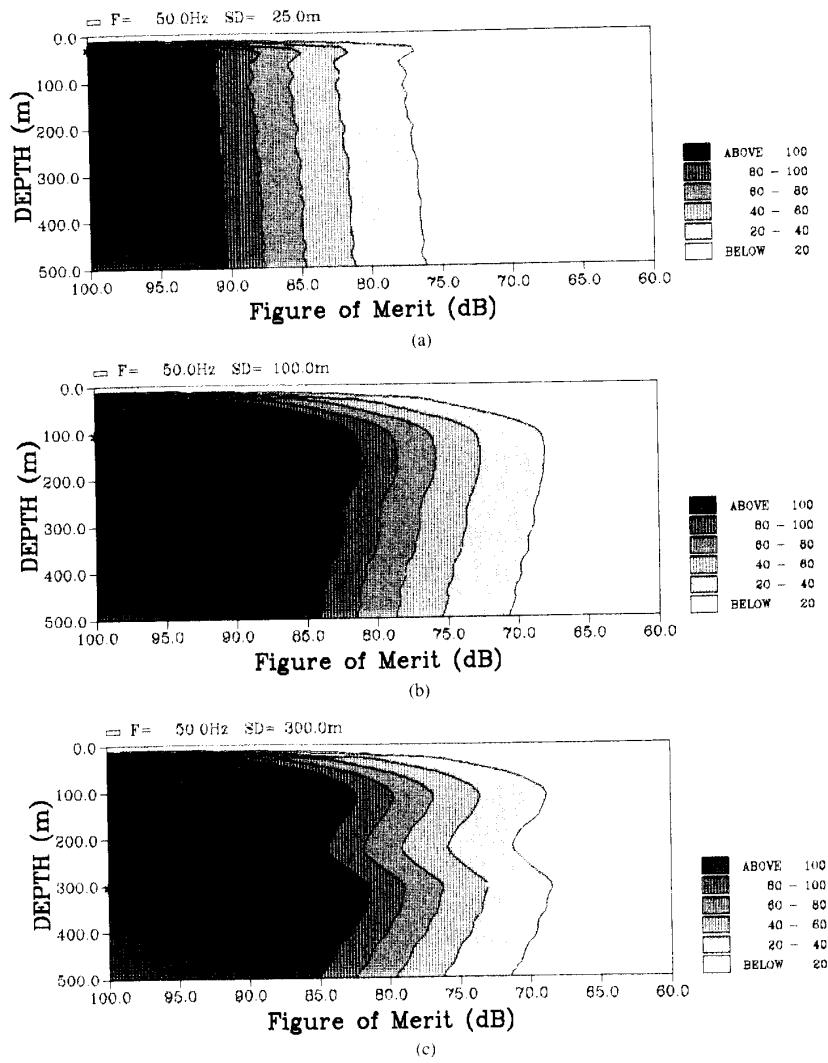


Fig. 7. Detection radius for the summer profile and a 50-Hz source at depths (a) 25 m, (b) 100 m, and (c) 300 m.

2.6. Interpretation

The occurrence of peaks in the detection radius at source and conjugate depths is an interesting feature that deserves some analysis, especially if we hope to comment on its generality. A fairly complete explanation of this feature is provided in a sequence of papers by Weston [5]-[7], which we briefly review.

In essence, there are three mechanisms that favor source and conjugate depths. First, there is a *ray windowing* effect. Whenever the sound speed is greater than that at the source, then some portion of the ray take-off angles is windowed. That is, some of the rays corresponding to shallow take-off angles are turned before reaching the receiver and therefore make no contribution. Conversely, when the receiver is at any depth where the sound speed is less than that at the source, then all rays emanating from the source will make a contribution to the range-averaged intensity. This is a direct

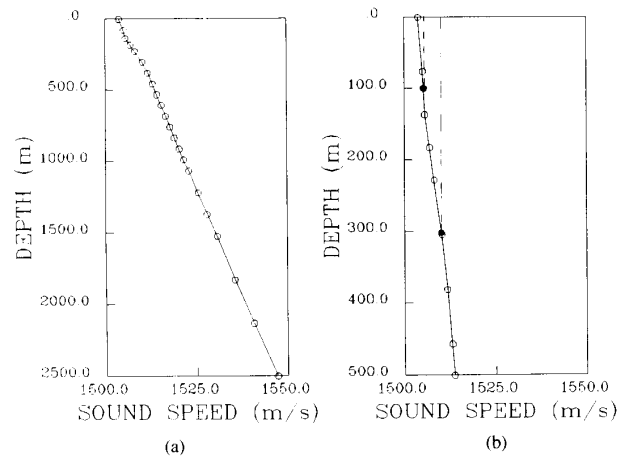


Fig. 8. Sound speed profile in the Mediterranean site during the winter (a) Full water column., (b) Blow-up of upper 500 m.

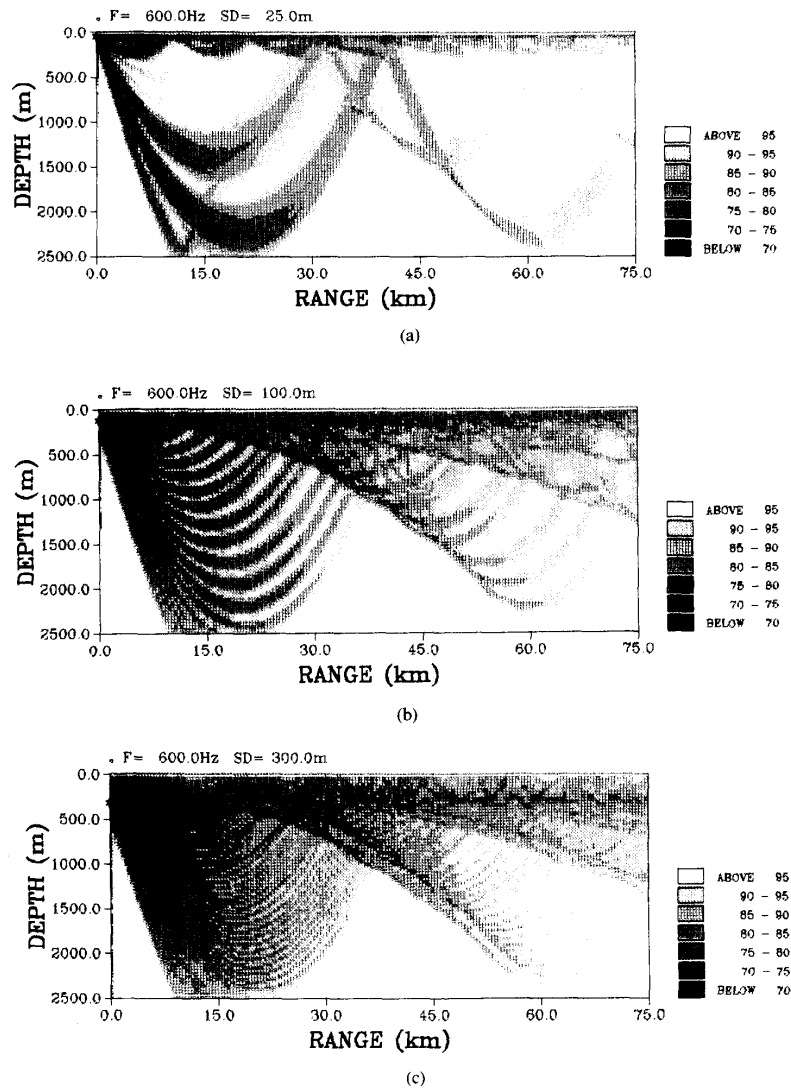


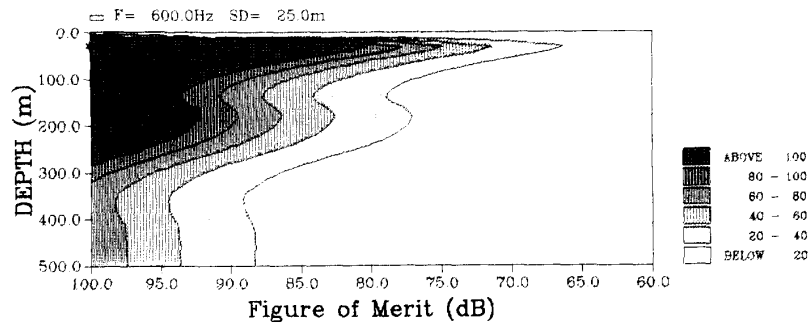
Fig. 9. Transmission loss plots for the winter profile and a 600-Hz source at depths (a) 25 m, (b) 100 m, and (c) 300 m.

consequence of Snell's law and is easily seen in the ray trace shown in Fig. 11 for the 300-m source depth. Note that all rays cycle through the depth between 60 m and 300 m where the sound speed is less than that at the source. As we move a receiver progressively deeper in depth, only the steeper ray take-off angles contribute.

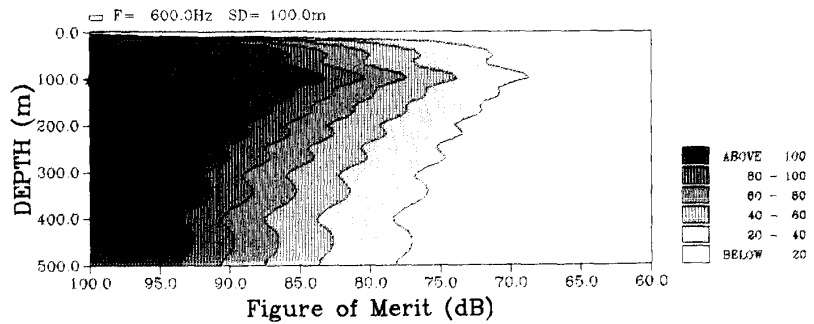
Secondly, there is a *ray tube projection* effect which, within the domain where the receiver sound speed is less than the source sound speed, favors those particular depths where the average ray angle at the receiver is shallowest. This in turn occurs when the receiver sound speed is the same as that at the source. Thus, if we consider a particular ray tube, then the intensity integrated across the ray tube is constant. If we then look at the intensity integrated along a line of constant

depth then that integral increases as the ray angle becomes shallower. (A simple explanation of the ray-windowing and ray projection effects may also be derived from modal theory.)

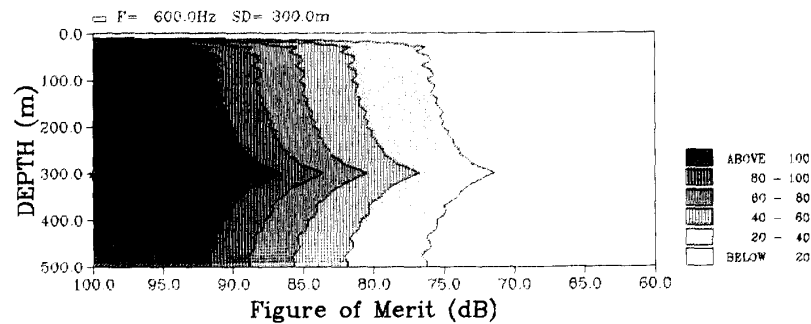
Finally, there is a *mode coupling* effect, which is distinguished from the first two mechanisms by not relying on a refractive mechanism. Thus, examining the ray trace for an isovelocity wave guide shown in Fig. 12, all rays emanating from the source contribute at any receiver depth; the rays follow straight-line paths and have no turning points in the water column. In addition, since the ray paths are straight, then the projection of the ray tube cross-sectional intensity on a constant receiver depth line is independent of receiver depth so that the second mechanism does not come into play.



(a)



(b)



(c)

Fig. 10. Detection radius for the winter profile and a 600-Hz source at depths (a) 25 m, (b) 100 m, and (c) 300 m.

Nevertheless, the detection radius plots shown in Fig. 13 manifest peaks at the source depth (and also at the complementary depth). Loosely speaking, a receiver at the same depth as the source provides a sort of matched filter in coupling well to modes that are well excited at the source. Other depths have some random weighting of modes, which is statistically a poorer match to those excited at the source. A more complete discussion may be found in [7].

The relative importance of these various mechanisms is not always easy to gauge. For low frequencies, steep bottom interacting rays, which are less affected by the refractive effects of the ocean, play an important role and can mask the first two effects. In addition, at very low frequencies we can set up a case where there is only one mode, in which case the

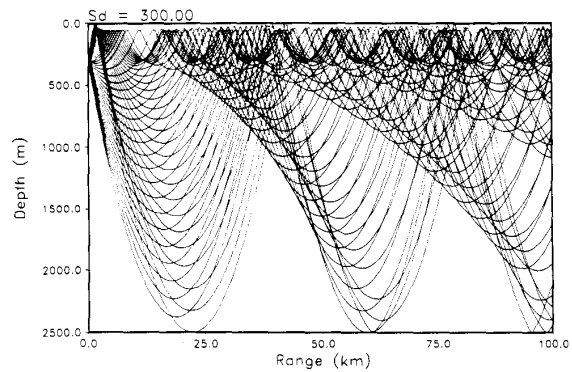


Fig. 11. Ray trace for summer profile.

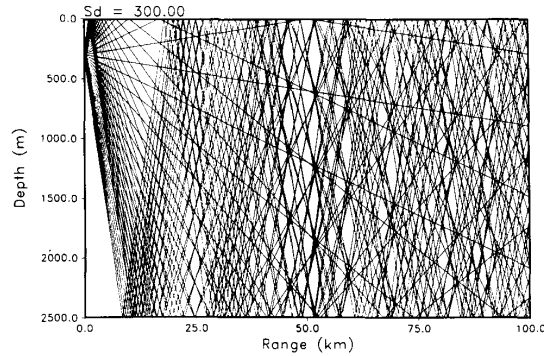


Fig. 12. Ray trace for the isovelocity profile.

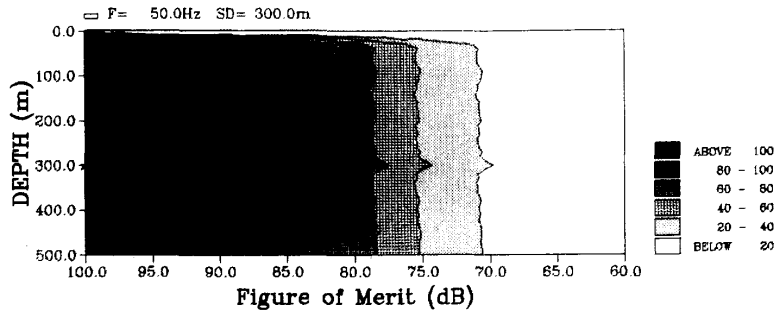


Fig. 13. Detection radius for the isovelocity profile.

optimal receiver depth will be at the mode peak regardless of source depth. We should also point out that the ray flux arguments implicitly assume that the ray cycle distance is short compared to some scale of intensity decay. Basically, this assumption is made when we compare intensity at different points in a ray cycle based on its projection and neglecting the overall cylindrical spreading loss. Thus, for example, a strong CZ pattern is associated with long cycle distances, so the argument is somewhat weakened.

Finally, when the source is within a few wavelengths of the surface, surface interference effects are important and the acoustic intensity falls off to zero as we approach the ocean surface. Shipping noise also falls off near the surface so that it is difficult to draw conclusions.

III. THE CASE OF UNKNOWN SOURCE DEPTH

The preceding discussion has assumed that the source depth was known. In the event that this information is lacking, then the previous rule of thumb is inapplicable. Some simple conclusions, however, can be obtained from the plots for the known source depth case by simply changing the interpretation. That is, by the principle of reciprocity, we can interchange the role of source and receiver. Then we may interpret our previous plots as representing the radius of detection for a fixed receiver depth plotted as a function of source depth. Thus, referring back to Fig. 5(a), we observe that a tow depth of 25 m yields poor performance for all source depths. By lowering the receiver to 100 m (Fig. 5(b))

we obtain much improved coverage for sources depths in the 50–500 m region. Note also that coverage of the shallow source is poor for each of the three tow depths.

In order to provide a somewhat more formal treatment we suppose that the source depth is known in a statistical sense. That is, that there is some probability density function, $p(z_s)$, which indicates the likelihood of the source being at some particular depth, z_s . We then compute the probability of detection for each of a number of source depths and take an average of the results to obtain a new probability of detection, $p_D^{(USD)}(r, z_r)$ (USD for unknown source depth). The average is done in a weighted sense; that is, we weight the individual probabilities of detection in proportion to the likelihood that the source is at that particular depth. Thus

$$p_D^{(USD)}(FM, r, z_r) = \int_0^\infty p(z_s) p_D(FM, r, z_r | z_s) d(z_s) \quad (5)$$

and then the detection radius is defined as before:

$$R^{(USD)}(FM, z_r) = \int_0^\infty P_D^{(USD)}(FM, r, z_r) dr. \quad (6)$$

Now, if $p(z_s) = \delta(z_s - z_0)$ —that is, if we know the source depth precisely—then the above formula gives the same result as before. In an opposite extreme we now

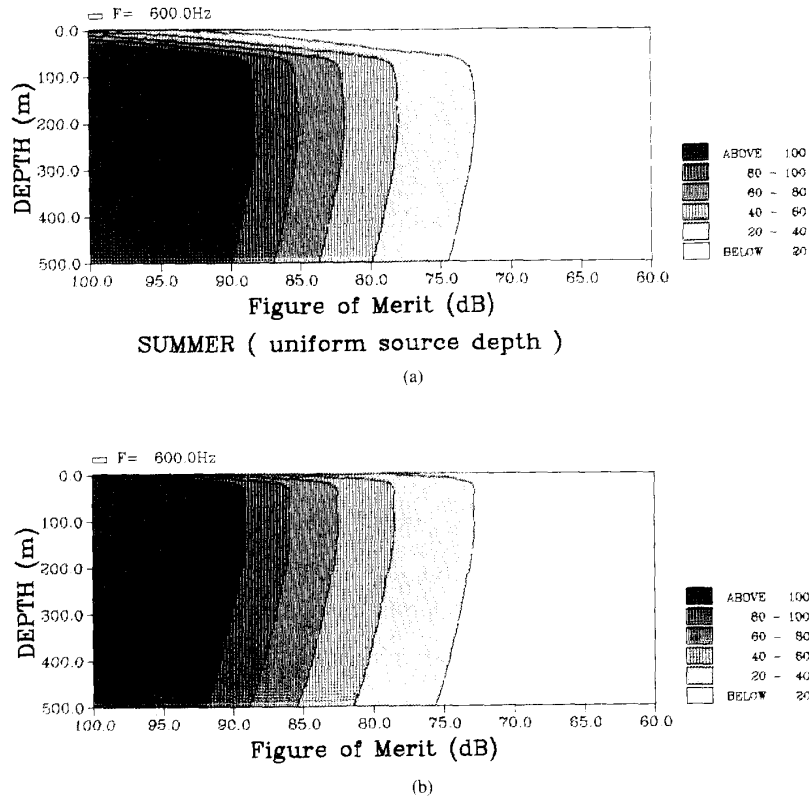


Fig. 14. Detection radius for the case unknown source depth for (a) summer and (b) winter.

consider

$$p(z_s) = \begin{cases} 1/500, & z_s \leq 500 \\ 0, & \text{else.} \end{cases} \quad (7)$$

In other words, we assume that all source depths between 0 and 500 m are equally likely. The results are indicated in Fig. 14 for both the summer and winter profiles. We observe that again there is a drop-off in detection radius for a receiver within a few wavelengths of the surface due to the surface interference effect. Apart from this feature the detection radius roughly images the sound speed profile, i.e., the detection radius is high when the sound speed is low and vice versa. This leads to the second rule-of-thumb: *when the source depth is unknown then the minimum sound speed depth is optimal*, i.e., the depth where the sound speed is as low as possible.

Again some interpretation is warranted. We recall from the previous section that a particular source depth yields a peak in detection radius at the same depth. The strength of that peak is in turn roughly inversely proportional to the sound speed at that depth because higher sound speeds imply a narrower window of *waterborne* rays emanating from the source. Thus in a first approximation the value of the uniform detection radius at any given depth is inversely proportional to the sound speed.

A complicating factor is that a given source depth also generates a peak at the conjugate depth. Again, the strength of this peak is inversely proportional to the sound speed so that we may still expect an image of the sound speed profile. However, not all source depths yield conjugate depths so the detection radius for a uniform distribution of source depths need not be a perfect image of the profile.

Note that the arguments for optimizing tow depth can equally well be interpreted from the point of view of picking a source depth to *minimize* the probability of detection. Thus, referring to Fig. 5(a), we see that a source at 25 m is very difficult to detect and so that depth might well be favored over deeper depths. (There are, of course, other complications in choosing a source depth.) Where such information is available it can easily be included in the calculations—one need only insert the correct form of $p(z_s)$ (or one's best guess) in the above equations. A real-time system might enable such a curve of the probability of a source being at a given depth to be input interactively.

IV. DISCUSSION

In the course of this study we have made numerous assumptions that affect the domain of applicability of the conclusions. In the following, we consider one by one some of the more important assumptions.

4.1. Depth-Independent Noise Background

In the first place, we note that flow-induced noise may vary as a function of tow-depth. In terms of ambient noise level, we expect significant depth dependence in regions where the sound speed exceeds that near the surface, for instance, below the critical depth in a deep-water scenario or throughout the water column in an Arctic scenario. In addition, the noise level due to distant shipping will decrease within a few wavelengths of the surface due to the surface decoupling effect. Of course, signal level decays rapidly as we approach the surface for the same reason.

Considering the 10–500-m region, i.e., the region of most relevance for towed arrays, it is much less clear what will happen. Results of some simple noise modeling for these Mediterranean profiles indicated that the noise level should be fairly flat as a function of receiver depth (to within a couple of dB). However, it is not at all clear whether this is a general result.

4.2. Depth-Independent Directivity Index

The array beam pattern using conventional planewave beamforming is affected by the multipath and refractive effects of the oceanic waveguide, especially towards endfire, and may provide depth-dependent array gain. Secondly, array deformation and thus array gain may vary as a function of array tow depth. Finally, bottom bounce and waterborne energy may be expected to differ in coherence, which loosely means that 3 dB of bottom bounce energy is not as good as 3 dB of waterborne energy. These three mechanisms may all provide depth-dependent array performance and affect our conclusions on optimal deployment depth.

4.3. Log-Normal Transition Curve

We have assumed a transition curve that varies in a log-normal manner with signal excess. Obviously, another factor is observation time, which leads to the so-called “ λ - σ ” model for the probability of detection. With regard to such embellishments, we observe that efforts to obtain values of λ and σ have apparently not been very successful [8]. In addition, the results seem to be somewhat insensitive to the shape of the transition curve: we have examined cases for $\sigma = 0$ and $\sigma = 10$ dB and found no significant changes in the results.

4.4. The Detection Radius

One of the difficult questions in optimizing tow depth is to precisely define what we mean by optimal. Maximizing the detection range is a reasonable criterion; however, detection range can be characterized in different ways, for instance, by the area covered with a 50% probability of detection, or by the maximum range for which some probability of detection threshold is attained.

We should like to single out one alternative for special consideration. We imagine an exaggerated convergence zone pattern in which there is absolutely no coverage except at a distance of, say, 50 km, at which point there is a very thin

ring of perfect coverage (the CZ). For the purposes of sweeping out an area this coverage pattern is just as good as if the thin ring extended from 0 to 50 km. That is, both a 50-km ring and a 50-km disk sweep out the same area. Our radius of detection, however, characterizes the disk coverage as vastly superior.

A modified *cumulative* radius of detection would compensate for this effect:

$$R(\text{FM}, z_r | z_s) = \int_0^\infty \max_{(r, \infty)} p_D(\text{FM}, r, z_r | z_s) dr. \quad (8)$$

Notice that the probability of detection has in effect been replaced by a function that increases monotonically as the source closes in range. In other words, the probability of detecting a source at a given range is redefined as the maximum of the single look probability of detection.

In environments where the probability of detection increases steadily as we close in range, obviously the cumulative radius of detection will be the same as what we had used earlier. In CZ propagation, however, the two schemes yield radically different numbers. In terms of the cases considered in this paper we can say that only Fig. 5(a) is significantly changed by using a cumulative radius of detection. Even then the shape of the curves is similar so that the conclusions about choosing the optimal depth are unchanged. The cumulative calculation however fails to take into account the role of integration time and so it too is somewhat misleading. In summary we can say that the cumulative and standard radius of detection provide bounds which for CZ propagation may be fairly coarse.

4.5. Range-Independent Environment

We have assumed a perfectly stratified or range-independent environment. Obviously this is never precisely true and for severely range-dependent problems our rules-of-thumb will no longer be valid. The machinery for calculating a radius of detection, however, remains valid with the substitution of a range-dependent or 3-dimensional propagation loss calculation.

V. CONCLUSIONS

In summary, the principal conclusions that emerge from this study are the following:

- If the source depth is known then the array should be deployed at that depth or at a conjugate depth, where the sound speed matches that at the source (source-depth/conjugate-depth rule).
- If the source depth is not known, then the array should be placed at a depth where the sound speed is as low as possible (minimum sound speed rule).

In both cases, a depth within a few wavelengths from the surface should be avoided because of the destructive interference of direct and surface reflected rays.

Following these rules can lead to as much as a tripling in detection radius or an increase of 10 dB or so in terms of the

quietest detectable source. (see for instance the summer curve for 600 Hz with a source depth of 100 m.) As discussed above, certain simplifying assumptions are implicit in these statements; nevertheless, we feel that they will be of value in most deep-water areas.

REFERENCES

- [1] D. A. Gershfeld and F. Ingenito, "Optimum depth of propagation in shallow water," Naval Research Laboratory Rep. 8741, 1983.
- [2] W. A. Kuperman and F. Ingenito, "Attenuation of the coherent component of sound propagating in shallow water with rough boundaries," *J. Acoust. Soc. Am.*, vol. 61, pp. 1178-1187, 1977.
- [3] F. B. Jensen and M. C. Ferla, "SNAP: the SACLANTCEN normal mode acoustic propagation model," in *SACLANTCEN SM-121*, La Spezia, Italy: SACLANT Under-sea Research Centre, 1979.
- [4] R. J. Urick, *Principles of Underwater Sound*, New York: McGraw-Hill, 1983.
- [5] D. E. Weston, "Acoustic flux formulas for range-dependent ocean ducts," *J. Acoust. Soc. Amer.*, vol. 68, pp. 269-281, 1980.
- [6] — "Wave-theory peaks in range-averaged channels of uniform sound velocity," *J. Acoust. Soc. Amer.*, vol. 68, pp. 282-286, 1980.
- [7] — "Acoustic flux method for oceanic guided waves," *J. Acoust. Soc. Amer.*, vol. 68, pp. 287-296, 1980.
- [8] S. Hanish, "Key issues in the application of statistics of acoustics fluctuations to system performance modeling," in *Pro. Acoustic Fluctuation Workshop*, S. Hanish *et al.*, Ed., 1979.



Carlo M. Ferla received the B.S. degree in information sciences in 1974 from the University of Pisa, Italy.

Since 1978 he has been employed by the SACLANT Undersea Research Centre as a senior scientist in the Environmental Modeling Group. He is responsible for the design and development of models for signal and noise propagation in ocean waveguides, as well as their application to modeling data from experiments at sea and in simulating sonar system performance.



Michael B. Porter received the B.S. degree in applied mathematics from the California Institute of Technology in 1979 and the Ph.D. degree in engineering science and applied mathematics from Northwestern University, Evanston, IL, in 1984.

From 1983 to 1985, he was with the Naval Ocean Systems Center, San Diego, CA. From 1985 to 1987 he was with the Naval Research Laboratory in Washington, DC. Since 1987, he has been at SACLANT Undersea Research Centre, La Spezia, Italy.

Dr. Porter is a member of the Acoustical Society of America and the Society for Industrial and Applied Mathematics.